CCUS: 4014874

CO2 Plume Imaging with Accelerated Deep Learning-based Data Assimilation Using Distributed Pressure and Temperature Measurements at the Illinois Basin-Decatur Carbon Sequestration Project

Takuto Sakai*[1], Masahiro Nagao[1], Chin Hsiang Chan[1], Akhil Datta-Gupta[1], 1. Texas A&M University.

Abstract

It is crucial to monitor the CO2 plume effectively throughout the life cycle of a geologic CO2 sequestration project to ensure safety and storage efficiency. However, the computational cost of existing data assimilation methods can be prohibitively expensive due to the complex physics with multi-component non-isothermal simulation and high dimensionality of large-scale reservoir models. We address this challenge by proposing an accelerated deep learning-based workflow for model calibration and prediction of CO2 plume evolution in the reservoir.

In the proposed workflow, a neural network model utilizes available monitoring data such as downhole pressure and temperature measurements as inputs and predicts the diffusive time of flight (DTOF) map as a representative reservoir image of the flow field. Reservoir model calibration can be implemented by selecting the ensemble of the training data samples that describes the predicted DTOF map. The computational efficiency of the framework is significantly enhanced in two ways. First, instead of using multiple CO2 saturation maps for different timesteps, a single DTOF map is used as the output image. The DTOF is the arrival time of pressure front propagation, which can be computed by the Fast Marching Method (FMM) rapidly without simulations. Since the reservoir dynamics is compressed into a single DTOF image, the memory and computational cost are reduced significantly. Second, an optimum coarsening of geologic model is applied, which substantially reduces the training data generation cost. The optimum coarsening scheme is utilized to maximize the computational time reduction and minimize the error of simulated monitoring data, such as well pressure and temperature data.

The power and efficacy of our workflow is demonstrated by application to the Illinois Basin-Decatur Project (IBDP), a large-scale CO2 storage test in saline aquifer. The data assimilation process is implemented

rapidly by the proposed workflow with given field measurements including distributed pressure and temperature sensing (DTS) data at an injection and a monitoring well. CO2 plume evolution is predicted by running the simulations of the calibrated reservoir models.

The proposed framework considerably speeds up the training data generation for machine learning, enabling rapid assimilation of distributed temperature and pressure data and CO2 plume imaging in large-scale CO2 storage reservoirs while including non-isothermal and compositional effects.

Introduction

Geological CO2 sequestration is known to be a critical technology to reduce anthropogenic greenhouse gas emission and decelerate the global warming (Michael et al. 2010, Sharma 2011, Viebahn et al. 2015, Zhou et al. 2016, Aminu et al. 2017). The injected CO2 needs to be securely isolated from the surrounding environment not only for preventing global warming, but also for securing groundwater and human health (Benson and Myer 2003, Wilkin and DiGiulio 2010). CO2 leakage may occur from legacy wells, natural fractures and faults (Song and Zhang 2013, Jia et al. 2018, Onishi et al. 2019). Properly understanding the reservoir structure and monitoring of CO2 migration is a crucial aspect of CO2 sequestration operation and risk management of CO2 leakage. However, traditional history matching workflow can be prohibitively expensive for the purpose of efficient and optimal reservoir management. The objective of this study is to propose an efficient data assimilation workflow using deep learning and to visualize CO2 plume evolution given monitoring data while properly considering the geological and fluid model uncertainties.

Full-physics numerical simulations for CO2 sequestration reservoirs usually involves millions of grid cells and complex physics such as multi-component non-isothermal fluid flow. Although traditional history matching workflow such as genetic algorithm is a widely used tool, it requires numerous simulations during the algorithm implementation, and it can be computationally prohibitive for field-scale history matching or optimization.

Reduced physics models are widely used to reduce the computational time of numerical simulation. Several analytical or semi-analytical solutions have been developed for estimating the CO2 plume migration (Nordbotten et al. 2005, Mathias et al. 2008) with an assumption of homogeneous reservoirs. The vertical equilibrium (VE) models are commonly used in CO2 storage applications that reduces the spatial dimension from 3D to 2D and associated computational cost (Møll Nilsen et al. 2011, Bandilla et al. 2014, Guo et al. 2014, Nilsen et al. 2016). A fast connectivity-based proxy was proposed by Jeong and Srinivasan (2016) to approximate CO2 plume migration in 3D heterogeneous reservoir. The fast-matching method (FMM)-based rapid simulation has been developed to significantly reduce the CPU cost via coordinate transformation from 3D to 1D (Zhang et al. 2016) or multi-domain multi-resolution upscaling (Chen et al. 2022) using the diffusive time-of-flight (DTOF) (Sethian 1999, Datta-Gupta et al. 2011). Iino et al. (2020) applied the FMM-based rapid simulation to unconventional shale reservoirs with CO2 huff ‘n’ puff considering multicomponent fluid flow, in which more than two orders of magnitude speed up is achieved. Streamline simulation is also a powerful tool to reduce the computational time. Tanaka et al. (2014) developed a 3-phase compositional streamline simulator and demonstrated its application to CO2 injection case. Streamline can also provide an efficient history matching workflow, which has been applied to CO2 injection problems (Vasco et al. 1999, Datta-Gupta and King 2007), for example, post-combustion CO2 water-alternating-gas (WAG) injection (Olalotiti-Lawal et al. 2019) and geologic CO2 sequestration in depleted oil reservoir (Yao et al. 2021).

Over the past few years, there are a lot of development related to machine learning technologies to predict CO2 plume evolution for CO2 injection problems. Chen et al. (2018) applied Multivariate Adaptive Regression Splines proxy model for the filtering-based data assimilation process to quantify uncertainty of CO2 leakage. A special type of Recurrent Neural Networks called Statistical Recurrent Unit (SRU) was applied to the routine well injection/production measurements to estimate the inter-well connectivity in post-combustion CO2 water-alternating-gas (WAG) injection reservoirs (Chen et al. 2021, Sen et al. 2022).

Convolutional Neural Networks (CNNs) is a key technology for image data prediction, and it is widely used for predicting the subsurface pressure and saturation distribution. Zhong et al. (2019) developed a conditional deep convolutional generative adversarial network (cDC-GAN) to predict CO2 plume migration in a heterogeneous reservoir with a single injection well. Mo et al. (2019) applied the deep convolutional encoder-decoder to CO2-water multiphase flow systems to predict snapshots of the CO2 saturation and pressure at different timesteps. Wen et al. (2021) proposed a residual U-Net (R-U-Net) based surrogate model to predict the CO2 plume migration under different permeability fields, injection history and injection location in a single injector scenario. Then, Tang, Liu, et al. (2021) extended the recurrent R-U-Net architecture so that it can predict 2D and 3D dynamic pressure and saturation. It was applied to oil production data assimilation problems with multiple producers and injectors scenarios. An efficient data assimilation and uncertainty quantification workflow was also developed by Tang, Fu, et al. (2021) to estimate the areal extent of CO2 plume, where R-U-Net was used to predict CO2 plume from permeability distribution and well location information. Fourier Neural Operator (FNO) is a cutting-edge machine learning technology, which was first applied to CO2 geological storage prediction by Wen, Li, Long, et al. (2022). This model substantially speeds up flow predictions compared with conventional numerical simulators. Wen, Li, Azizzadenesheli, et al. (2022) further extended this model to U-FNO for superior accuracy, speed, and data efficiency by combining U-Net architecture and FNO. The physics informed machine learning (PIML) framework has also been applied to CO2 sequestration modelling and reservoir engineering problems (Shokouhi et al. 2021, Yan et al. 2021, Nagao, Datta-Gupta, et al. 2023). Nagao, Datta-Gupta, et al. (2023) applied Physics Informed Neural Network (PINN) model for identifying reservoir connectivity and predicting production rate from historical well data such as injection/production and pressure data. Despite the widespread use of machine learning-based methods for CO2 sequestration problems in recent years, it has seen limited range of applicability, for example, two phase black oil type problem in 2D or simple 3D reservoir cases(Onishi et al. 2021). The challenge here is to develop a scalable workflow for field applications, which can properly handle associated complexities and computational burden in efficient manner.

In this study, we propose a deep learning-based workflow for data assimilation and CO2 plume visualization from available monitoring data, such as the injector bottom-hole pressure (BHP), the behind-casing distributed pressure data at a monitoring well, and DTS data along wells. This workflow was originally proposed by Onishi et al. (2021) for unconventional reservoir application and extended to adapt to applications of CO2 sequestration (Nagao 2022, Nagao et al. 2022, Nagao, Yao, et al. 2023). In this study, DTOF maps are used for input and output of variational autoencoder (VAE) instead of CO2 onset time maps which are used in the previous work. The use of DTOF can significantly reduce the computational time of training data generation because DTOF maps can be generated by FMM without simulations and in just a few seconds. In contrast, CO2 onset time map is created based on full-physics numerical simulations. Furthermore, we applied an optimal coarsening of geologic model to reduce the computational time of forward simulations, which significantly reduces the training data generation cost. The effectiveness and robustness of the proposed workflow will be demonstrated using the application to a large-scale CO2 storage test site.

Methodology

In this section, we introduce the proposed deep learning-based history matching workflow. We consider the situation where some monitoring data is available in the CO2 sequestration sites such as temperature and pressure measurements at wellbores.

First, we develop a data-driven neural network model to predict the subsurface pressure front propagation images in terms of DTOF given the monitoring data while considering the geological and fluid model uncertainties (**Figure 1**). Most of the existing machine learning-based proxy models predicts snapshots of pressure and saturation distribution in the reservoirs for all timesteps. Due to the high dimensionality of the reservoir model, the spatio and temporal distribution of pressure and saturation consumes extremely large

memory, which makes large-scale field application infeasible. Instead of storing pressure and saturation maps of every timestep, a DTOF map compresses snapshots of multiple pressure distribution images into a single image representing pressure front propagation (Sethian 1999, Datta-Gupta et al. 2011). Furthermore, DTOF images can be provided without running numerical simulation. One of the drawbacks of using pressure and saturation as outputs of proxy models is the computational cost for training data generation. It is required to run hundreds of full-physics numerical simulation for obtaining pressure and saturation images for all timesteps. For CO2 storage applications, non-isothermal and compositional simulations should be used to properly consider thermal effect and multi-component fluid behavior accurately. In such a case, the computational cost of numerical simulation becomes very expensive. However, DTOF images are calculated solely based on geologic properties and fluid properties at initial condition, and it can be calculated very efficiently using FMM. Use of DTOF significantly reduces the dimension of the problem and simplify the neural network architecture. As a result, it considerably enhances the efficiency of the whole workflow, enabling large-scale field application efficiently.

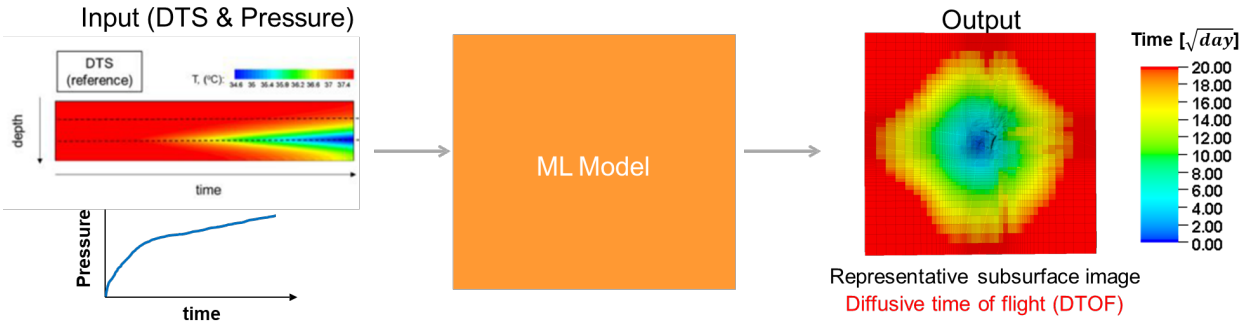

Figure 1. Proposed machine learning model for predicting DTOF images.

Next, we utilize the predicted DTOF image based on field monitoring data as a representative subsurface image for history matching purpose. Within the ensemble of training dataset, we select several nearest neighbor samples that have similar DTOF images with the predicted DTOF image, and these samples are considered as history matched reservoir models. Detailed workflow of the nearest neighbor model selection is discussed later in this section.

Neural network training and prediction of DTOF images

In our study, the VAE is used to compress the high dimensional DTOF images into low dimensional latent space. VAE was originally proposed by Kingma and Welling (2013), and the idea is to combine the concept from classical autoencoder and Bayesian inference. A classical autoencoder takes an image data as input, maps it to low dimensional latent space, and then decodes it back to original image dimension. Such classical autoencoder is built for the purpose of dimensionality reduction, and it sometimes does not lead to particularly useful or nicely structured latent space representation especially for highly nonlinear problems. On the other hand, the VAE augments autoencoders with a statistical process, forcing them to learn continuous and highly structured latent spaces. **Figure 2** shows the architecture of VAE. The input images are compressed into a fixed low dimensional latent space, providing two variables: mean and variance. VAE then calculates the latent variables by sampling from the normal distribution based on the given mean and variance. Then, it is decoded back to original image dimension. The sampling process forces the latent space to encode meaningful representation everywhere. This specific feature of VAE is very useful to properly account for the uncertainty of the predicted images. In our applications, the trained neural network can provide multiple predictions of DTOF image while considering the uncertainties associated with pressure front propagation. The VAE has the following loss function:

$$L_{VAE} = \frac{1}{N_x}\sum_{i=1}^{N_x}|x_i - \hat{x}_i|^2 - \frac{1}{N_z}\sum_{j=1}^{N_z}\frac{1}{2}\left[1 + ln(\sigma_j^2) - \sigma_j^2 - \mu_j^2\right] \quad (1)$$

where, x_i is the normalized pixel of DTOF images, $\hat{x}_i$ is the reconstructed pixel of the images, μ_j is the mean and σ_j^2 is the variance of the latent variables, N_x is the number of the image dimension and N_z is the latent space dimension. The first term is reconstruction loss that has same formula with classical autoencoder. The second term is called Kullback-Leibler (KL) divergence that enforce the distribution close to standard normal distribution, which has mean of 0 and variance of 1, to enforce continuous latent space representation.

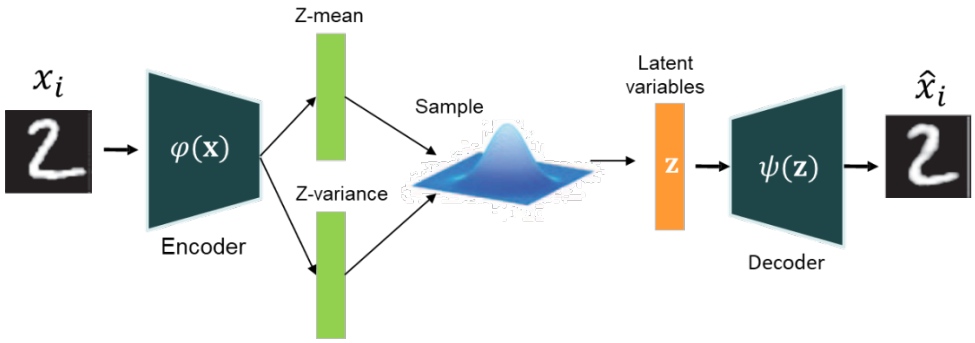

Figure 2. Schematic of the VAE architecture

The steps of the proposed deep learning-based workflow are given below and in **Figure 3**.

- The first step of the workflow is data generation for the neural network training. A sensitivity analysis is conducted to identify the influential parameters on the observed data, such as pressure and temperature measurements at wells. Next, the selected key uncertain parameters are sampled using Latin Hypercube sampling algorithm to generate an ensemble of reservoir model realizations to cover the uncertainty space. In this study, Eclipse™ commercial reservoir simulator is used to run simulations of the created ensemble and generate simulated monitoring data. The DTOF images are efficiently calculated by FMM without running simulations.
- The second step is the neural network training using the generated training dataset. The collected samples are divided into training, validation and testing dataset. The proposed neural network architecture is composed of two elements; CNN-based VAE to compress the high dimensional DTOF images into low dimensional latent variables and regression model to estimate the compressed latent variables from the available monitoring data such as DTS and pressure measurements. In the regression model, 2D CNN is used for image data with spatial information such as DTS data, and feed-forward neural networks is used for point measurements such as pressure measurements. These two parts of the neural network (VAE and regression model) can be combined and trained together. The loss function for the proposed neural network for each sample can be written as:

$$L = L_{VAE} + \frac{1}{N_z}\sum_{j=1}^{N_z}\left|\sigma_j^2 - \hat{\sigma}_j^2\right|^2 + \frac{1}{N_z}\sum_{j=1}^{N_z}\left|\mu_j - \hat{\mu}_j\right|^2 \quad (2)$$

where, μ_j is the mean and σ_j^2 is the variance of the latent variables calculated from the encoder network, $\hat{\mu}_j$ and $\hat{\sigma}_j^2$ are the predicted values from the regression model, N_z is the latent space dimension. The input data (DTOF, DTS and pressure measurements) are scaled using min-max scaler for neural network to train properly.

- The trained neural network is then used for the prediction of DTOF images given monitoring data. The field monitoring measurements are fed into the trained regression model, and the latent variables are predicted. Then, the trained decoder network maps the latent variables back to the original image dimension, which is the predicted DTOF map. Since the VAE is used in this study, multiple images can be provided considering the uncertainties of the predicted images.

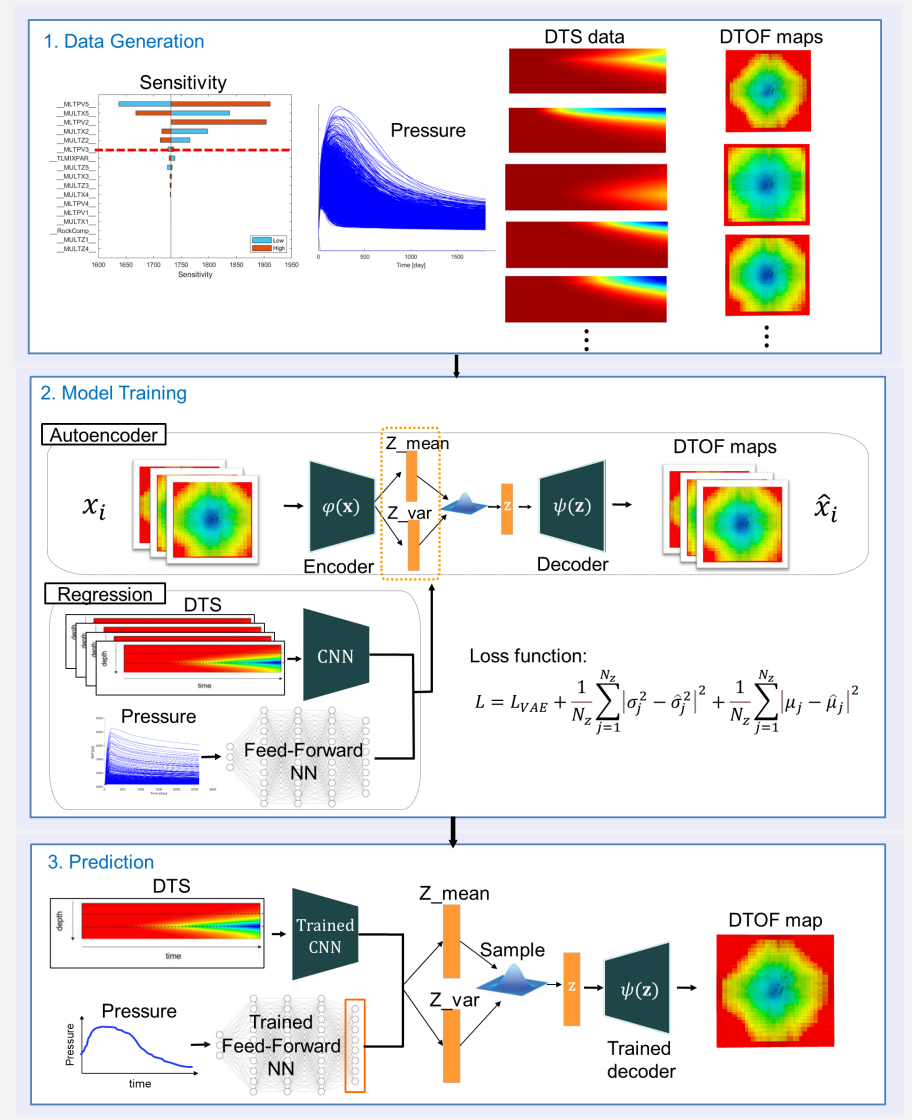

Figure 3. Workflow of the proposed deep learning-based subsurface image prediction

History matching using trained model

Once the neural network is successfully trained, it can be used for reservoir model calibration and prediction of the CO2 plume migration. One of useful features of VAE latent space is that the distance between the sample points represents the dissimilarity of those samples. It means that if two samples are far from each other, those two samples have very different DTOF images. In contrast, if two samples are close to each other, those two samples have very similar DTOF images. **Figure 4** shows the illustration of the VAE latent space representation. The generated training samples of DTOF images are compressed into the VAE latent space during the neural network training. The light blue symbol represents the training data samples mapped into the VAE latent space. For the reservoir model calibration in this framework, we first estimate the target latent variable using the trained regression model with given field monitoring data, such as well pressure and DTS measurements. In **Figure 4**, the target latent variable is expressed as a black cross. Since the distance becomes a measurement of dissimilarity in the VAE latent space, nearest neighbor samples to the target point have similar DTOF maps to the predicted DTOF map based on field monitoring measurements. The DTOF maps can be considered as a representative subsurface image that takes account of geologic model, fluid properties, and well location. Thus, the nearest neighbor samples can be considered as ensemble of calibrated reservoir models that captures the field monitoring data. By running forward simulations of the selected nearest neighbor models, we can predict the future CO2 plume migration.

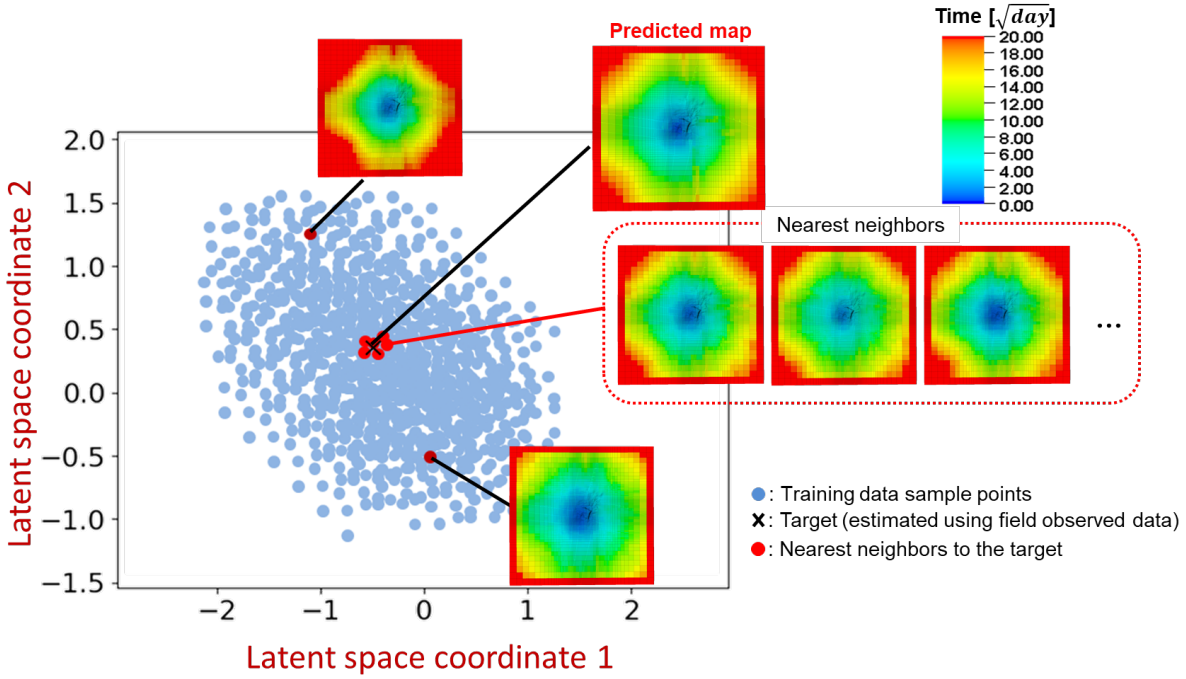

Figure 4. Illustration of the latent space representation for model selection and reservoir calibration

Field Application

In this section, the proposed deep learning-based workflow is applied to a large-scale CO2 sequestration project to show its effectiveness and versatility.

Project overview and model description

The Illinois Basin – Decatur Project (IBDP) is headed by the Midwest Geological Sequestration Consortium (MGSC), a federally funded regional partnership through the U. S. Department of Energy's National Energy Technology Laboratory (DOE). MGSC collaborates with Archer Daniels Midland (ADM) Company, Schlumberger Carbon Services, Trimeric, and other subcontractors, and the goal of this project is to inject 1 million metric tons of CO2 into a saline aquifer in Decatur, Illinois (**Figure 5**). There is an injector (CCS1)

and a monitoring well (VW1) in this field. CO2 injection operation commenced in November 2011, and it continued for three years at an approximate rate of 1,000 metric tons per day. This is one of the earliest large-scale CO2 storage project within the seven DOE Regional Carbon Sequestration Partnership. The second project called Industrial Carbon Capture and Storage (ICCS) is started from 2017 at the same site, and new injection well and monitoring well (CC2 and VW2) are completed for this project. Note that these wells are not included in the scope of this paper.

Figure 5. Location and description of the IBDP site (Wade Zaluski 2021).

The static model was built based on seismic survey, geophysical logs, and core analysis (Wade Zaluski 2021). As shown in **Figure 6**, the static model composed of eleven zones, and the main injection zone is Mt. Simon A-lower. As observed data, behind casing pressure at six different depth (WB1 to WB6) along the monitoring well, bottom hole pressure at the injector, and DTS data along the injector are available, which are shown in **Figure 7**. Since the injected CO2 temperature is higher than the temperature of the formation, an increase of temperature is observed at the injection zone in the DTS data.

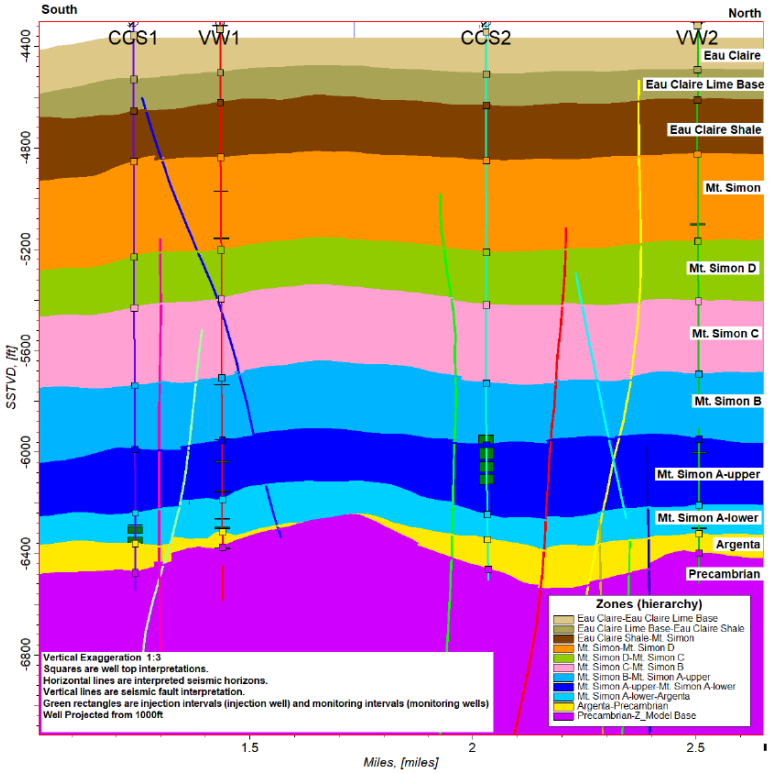

Figure 6. Description of geological zones of IBDP (Wade Zaluski 2021).

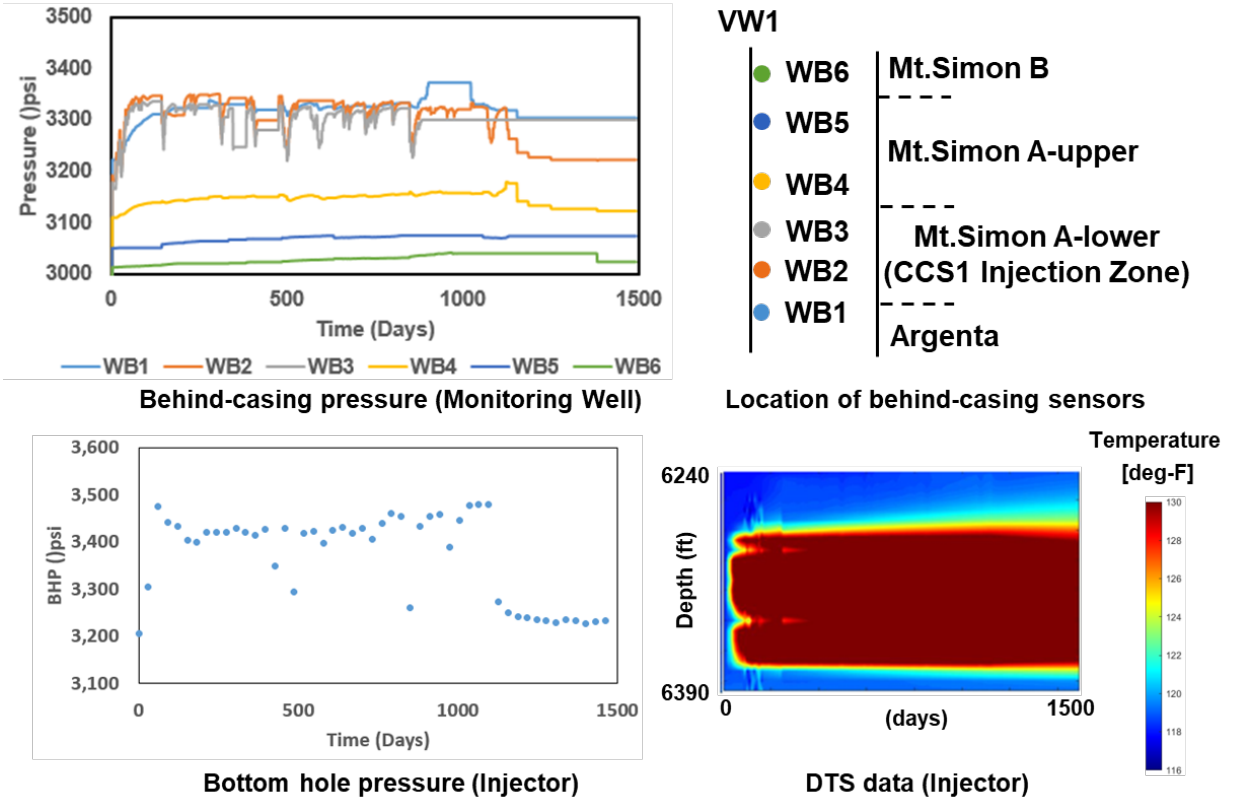

Figure 7. Available monitoring data for the IBDP site.

A part of the static model covering 9.7 miles x 9.3 miles are extracted as the dynamic reservoir model which has 126x125x110 dimension, in total 1.73 million cells. The lateral grid size is same as the static model and the smallest grid size around wells is 125 ft x 125 ft. The initial pressure distribution is from 2159 [psi] at the top layer to 4006 [psi] at the bottom layer. The permeability distribution is shown in **Figure 8**, which ranges from 1e-5 to 1683.9 [mD], and it has high heterogeneity. As stated, the main target zone for CO2 injection is Mt. Simon A-lower (middle layers in dynamic model) which has relatively high permeability. The injection schedule is shown in **Figure 9**, which is used as a constraint of the injector during the simulation. ECLIPSE 300 (compositional model) with CO2STORE module (three components: CO2, H2O, and NaCL) and thermal option is used. In this application, the proposed workflow is applied to visualize DTOF map and calibrate the reservoir model using the latent space representation of the trained neural network model.

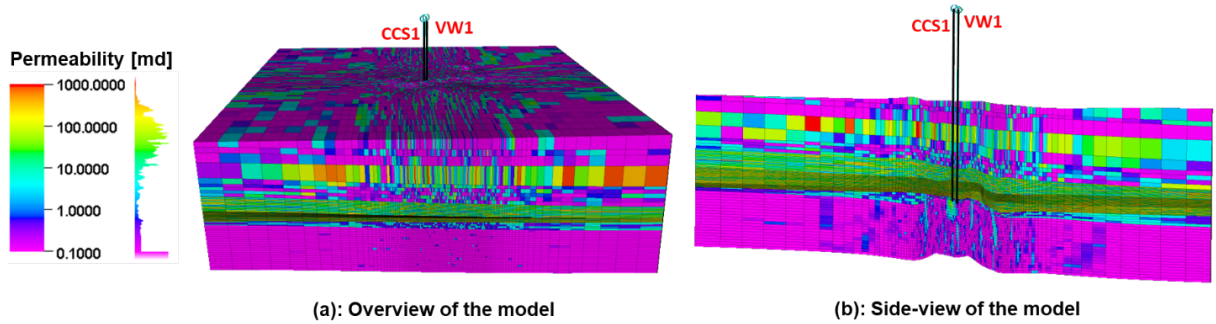

Figure 8. IBDP dynamic model (Permeability).

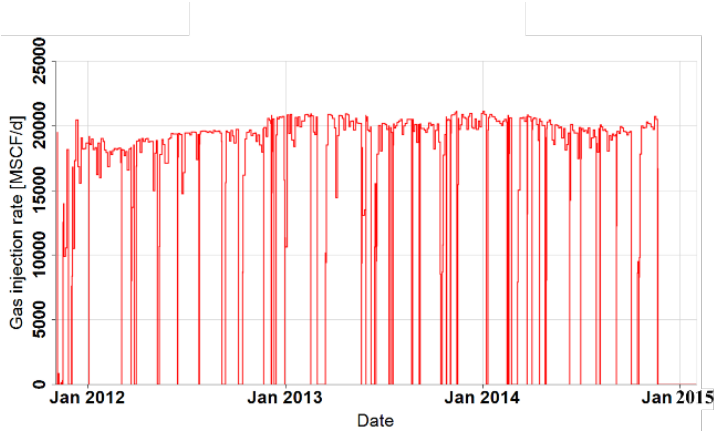

Figure 9. Injection schedule history.

Upscaling reservoir model to accelerate forward simulation and training

Since it is required to properly consider non-isothermal and multicomponent fluid flow for CO2 storage applications, and the IBDP model is a large-scale reservoir model, the simulation consumes significant computational resources. A single simulation requires approximately 600 hours for four years simulation. In this case, it is not feasible to run hundreds of simulations for training data generation. To mitigate the expensive simulation costs, we have implemented a model upscaling strategy and the injection schedule averaging to reduce simulation timestep. The details of the model coarsening strategy is illustrated in **Figure 10**. Our approach incorporates techniques of areal upscaling and vertical upscaling.

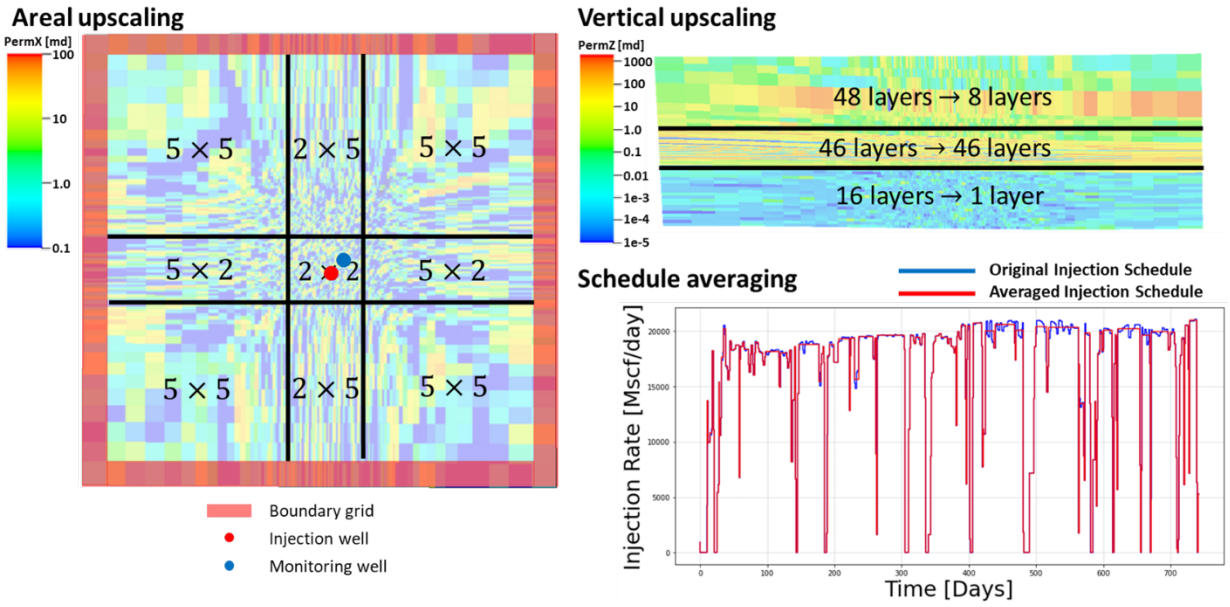

Figure 10. Illustration of upscaling methods and injection schedule averaging.

The IBDP model has a tartan grid, characterized by finer gridding near wells and coarser gridding in areas distant from wells. In the areal upscaling process, varying coarsening schemes are applied across different regions of the reservoir: 2x2 coarsening is utilized in areas near the wells, which covers the entire CO2 plume at the end of the operation. For the outside four regions, more aggressive 5x5 coarsening is adopted. To prevent the additional non-neighbor connections, 5x2 or 2x5 coarsening are implemented in the remaining four areas as shown in **Figure 10**. Additionally, IBDP model incorporates an infinite-acting boundary condition by assigning large pore volume multiplier to the boundary cells. To maintain the boundary, areal upscaling is applied excluding these boundary cells. In the vertical upscaling process, the

injection zone is kept as its original scale, while the zones above and below have aggressive upscaling scheme. Specifically, the bottom zone has the most aggressive upscaling due to its negligible impact on pressure behavior, as it does not have pressure gauge at this depth along the monitoring well and is separated from the middle zone by baffles. DTOF map can be generated by FMM without numerical simulations and the numerical simulations are needed only for generating monitoring data such as bottom hole pressure and DTS data. Since it is easier to maintain the accurate monitoring data than to maintain accurate grid pressure or saturation for all timesteps after coarsening, we can perform such active coarsening scheme.
In addition to upscaling, the injection schedule has been averaged. Originally, the schedule was set to report on a daily basis. This high reporting frequency prevented larger time steps, and it increased the computational cost. We reduced the number of timesteps by averaging the injection schedule. The averaged injection schedule is shown in **Figure 10** and closely resembles the original schedule.
Figure 11 shows the comparison of simulated well response data between the fine and upscaled model. It is confirmed that the upscaled model provide reasonable accuracy in terms of well pressure and DTS data. The upscaled model significantly reduces the computational time. Running the original fine-scale model on an Intel® Xeon® Gold 6226R CPU @ 2.90 GHz with 32 cores requires approximately 18 hours, which equates to roughly 600 hours on a single core. In contrast, the upscaled model requires only 7.1 hours under identical conditions with a single core, demonstrating a substantial reduction in simulation time.

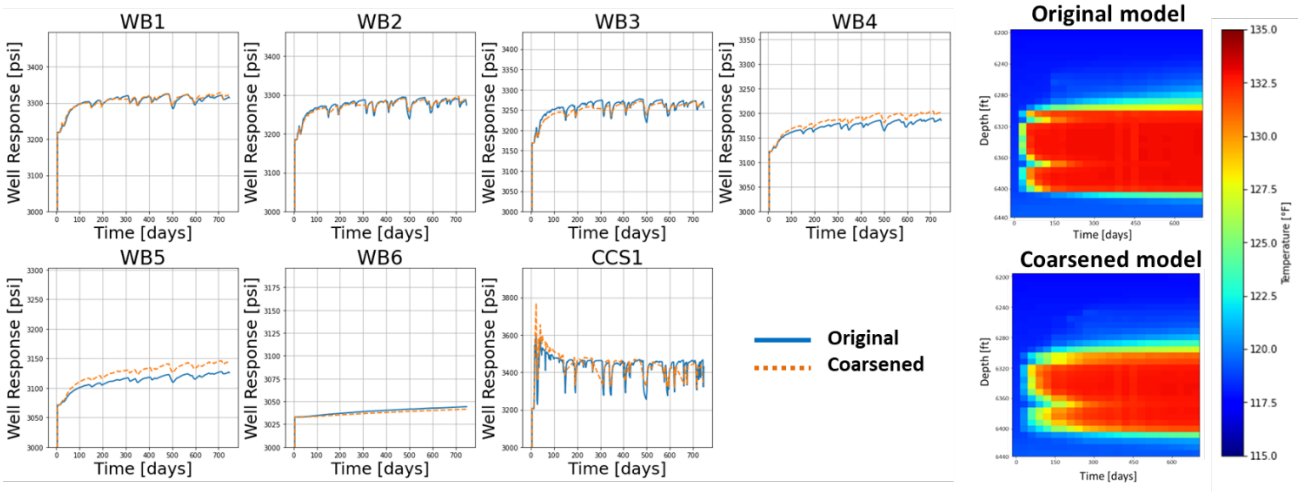

Figure 11. Comparison of well responses between original fine-scale model and coarse-scale models.

Parameter selection and sensitivity analysis
In this section, we describe the workflow of the parameter selection for training data generation. We first implement sensitivity analysis to identify the uncertain parameters that have large influence on the observed data, including pressure and DTS data. The regional definition is used for the geological property calibration, such as transmissibility and pore volume. Based on the underlying geological feature (**Figure 6**), the IBDP reservoir model is divided into four regions as shown in **Figure 12**. The pore volume multiplier and transmissibility multiplier for each region are included in the sensitivity analysis. In addition to that, rock compressibility, rock heat capacity, and thermal conductivity for the entire reservoir are included as parameters for sensitivity analysis. In this study, multiphase flow parameters such as end points of relative permeability curve or capillary pressure are not included in parameters for sensitivity analysis, although these parameters might be influential to the observed data. The investigation of these parameters are left for future work.

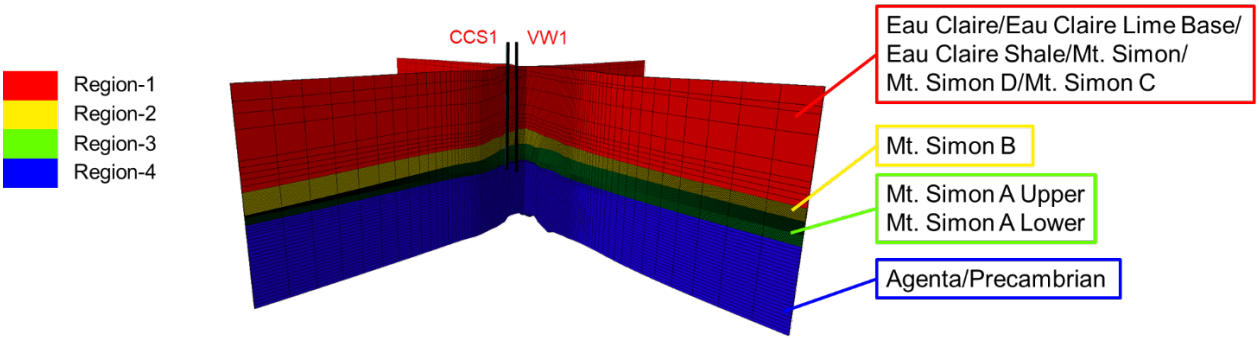

Figure 12. IBDP region definition.

Table 1 shows the list of parameters used for sensitivity analysis and their respective assigned range. One-variable-at-a-time design is used in this study. **Figure 13** shows the tornado charts created for each objective function (DTS data along injector, BHP of injector, and behind casing pressure of monitoring well). In **Figure 13**, the base case is indicated as vertical line whose horizontal axis is 0, and the differences of each objective function from base case is indicated as bar along horizontal axis. The difference generated by changing each parameter to 'Low' is indicated as blue, and the difference generated by changing each parameter to 'High' is indicated as red. Based on the results of sensitivity analysis, the six highly sensitive parameters are detected, including MULTZ1, MLTPV3, MULTX3, MULTZ3, MLTPV4, and THCON. In the training data generation, these detected parameters are changed within the specified uncertainty range, respectively, and 500 training data samples are generated.

Table 1. List of parameters used for sensitivity analysis and their respective assigned bounds.

Properties	Parameters	Description	Low	Base	High
Region Pore Volume Multipliers	MLTPV1	Region 1 PV Multiplier	0.7	1.0	1.3
	MLTPV2	Region 2 PV Multiplier	0.7	1.0	1.3
	MLTPV3	Region 3 PV Multiplier	0.7	1.0	1.3
	MLTPV4	Region 4 PV Multiplier	0.7	1.0	1.3
Region TRANX Multipliers	MULTX1	Region 1 TRANX Multiplier	0.5	1.0	2.0
	MULTX2	Region 2 TRANX Multiplier	0.5	1.0	2.0
	MULTX3	Region 3 TRANX Multiplier	0.5	1.0	2.0
	MULTX4	Region 4 TRANX Multiplier	0.5	1.0	2.0
Region TRANZ Multipliers	MULTZ1	Region 1 TRANZ Multiplier	0.1	0.5	1.0
	MULTZ2	Region 2 TRANZ Multiplier	0.1	0.5	1.0
	MULTZ3	Region 3 TRANZ Multiplier	0.1	0.5	1.0
	MULTZ4	Region 4 TRANZ Multiplier	0.1	0.5	1.0
Rock Compressibility	ROCK	Rock Compressibility (psi^{-1})	2.7E-06	3.2E-06	3.7E-06
Rock Heat Capacity	HEATCR	Rock Volumetric Heat Capacity (Btu/ft^3/deg-R)	0.3	0.5	0.7
Thermal Conductivity	THCONR	Combined rock and fluid thermal conductivity (Btu/ft/day/deg-R)	1.0	2.0	3.0

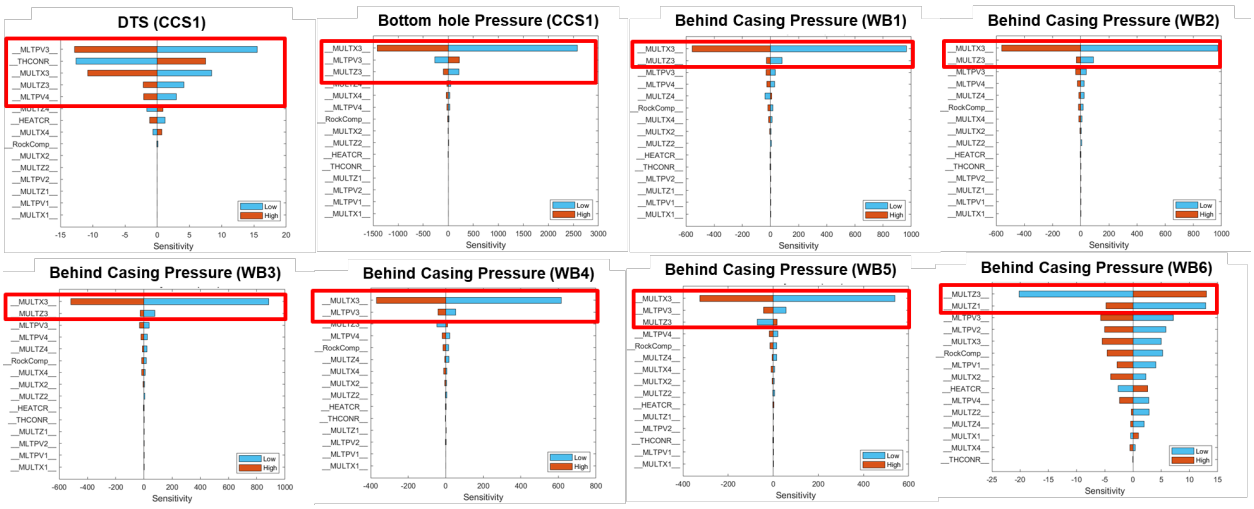

Figure 13. Results of sensitivity analysis.

Dataset generation and neural network training

In this section, we describe the workflow of the dataset generation and neural network training. The Latin hypercube sampling was applied to the selected six parameters during the sensitivity analysis, and 500 realizations are generated for neural network training. Using the 500 realizations, the DTOF maps are generated using FMM. Fine-scale reservoir model is used for the DTOF calculation, since it does not require numerical simulation in FMM. The numerical simulations of upscaled models were performed using a commercial simulator. Eclipse^{TM} (E300) (compositional simulator) with CO2STORE module is used for the simulation. After each simulation, the BHP of injector, the behind-casing pressure along the monitoring well, and the DTS data along injector are saved as training data. **Figure 14** and **Figure 15** show examples of generated training data. It is found that observed BHP/behind-casing pressure are covered by the generated pressure responses properly. Since the three pressure gages along the monitoring well, WB4, WB5, and WB6 are placed outside of the injection zone, these pressure data are excluded from the neural network training process. The generated 500 samples are divided into training (350), validation (75) and testing (75) samples. The neural network is built to predict DTOF map from the well pressure response and DTS data. **Figure 16** describes the overall architecture of neural network models. CNN-based VAE is used for image (DTOF map) compression, and CNN (for DTS data) and feed-forward neural network (for well pressure response) are used as regression model.

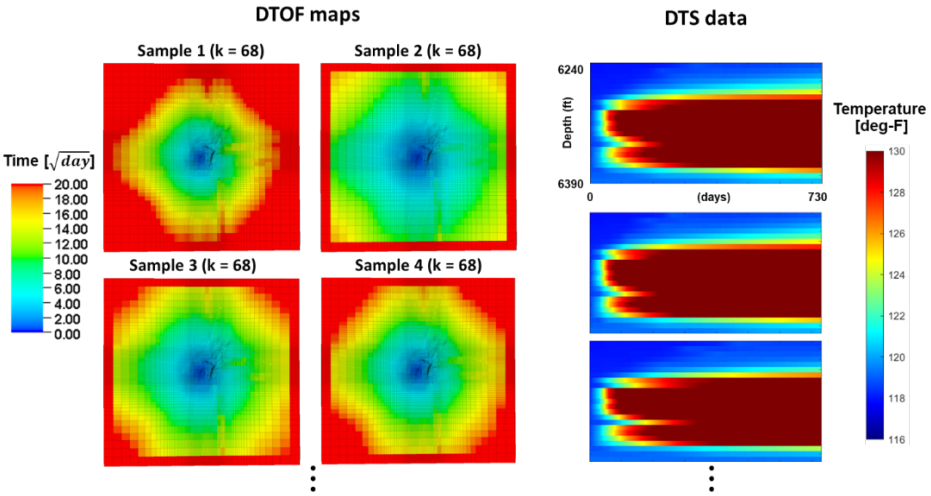

Figure 14. Examples of generated training data (DTOF maps and DTS data).

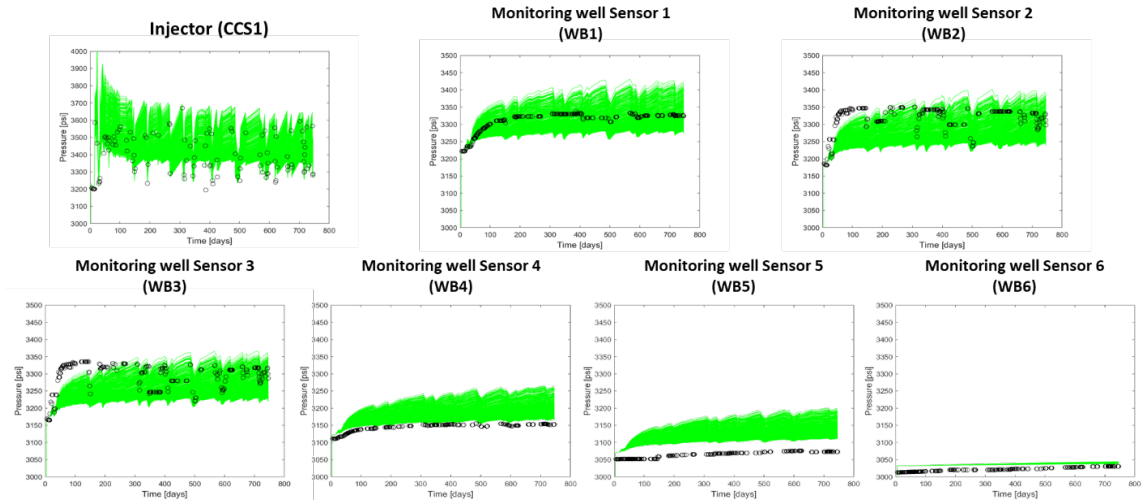

Figure 15. Examples of generated training data (pressure responses).

For the VAE part, 3D CNNs are used because DTOF map is 3D image, and 2D CNNs are used for the DTS data because it is a 2D image. The training condition of neural network is summarized in

Table 2 The runtime for the training was approximately 5 hours using GPU in Google Collaboratory. **Figure 16** also shows the training performance. The blue curve is the loss function of training dataset, and the orange curve is the loss function of validation dataset. The steady reduction trend of loss function can be observed in both training and validation datasets, indicating that the neural network training is successful. In this procedure, Tensorflow library in Python was used.

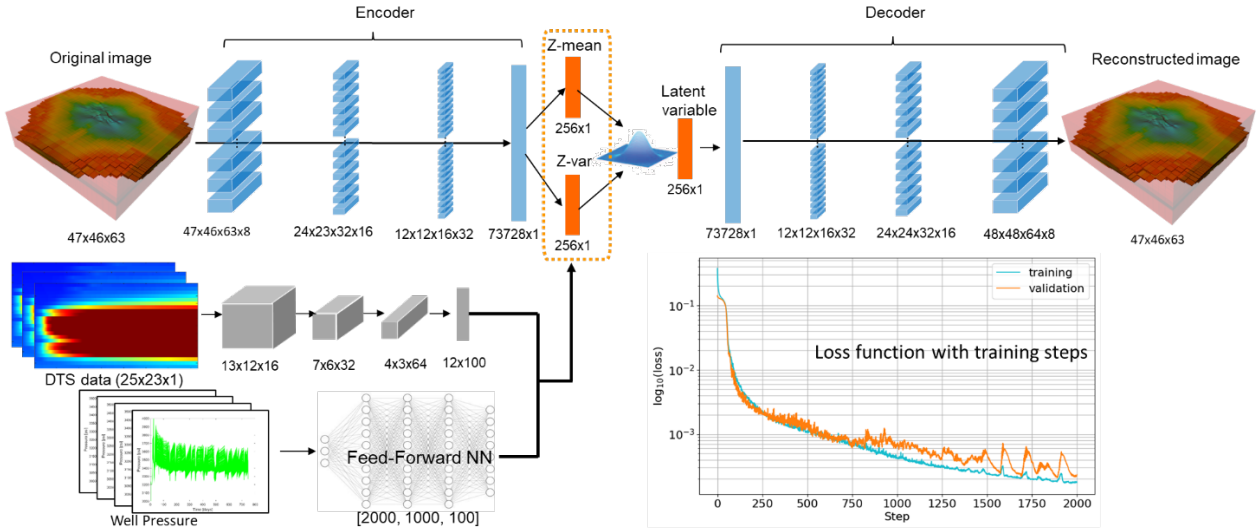

Figure 16. Overall architectures of neural networks for training and training performance.

Table 2. Neural network training conditions.

Conditions	Value
Batch size	200
Maximum number of epochs	2000
Patience	500
Optimizer	Adaptive Moment Estimation (ADAM) (Kingma and Ba 2014)
Initial learning rate	0.0001

Blind test of Diffusive-Time-of-Flight

After the neural network training, the prediction performance of DTOF maps given pressure response and DTS data was verified using the test samples. **Figure 17** shows the schematic of the neural network architecture for prediction of the DTOF maps. The DTS data and well pressure responses are fed into the trained regression model (trained CNN and trained feed forward NN), and it predicts the DTOF maps. The three randomly selected test samples out of 75 are shown in **Figure 18**. Since the characteristics of VAE enables to provide multiple predicted images considering the uncertainty of predicted images, three predicted images for each sample are provided in **Figure 18**. The prediction accuracy of the trained neural network model is validated, while properly considering the uncertainties of the predicted images. This blind test reveals that the trained neural network can successfully provide the DTOF map based on the monitored pressure responses at wells and DTS data along the injector.

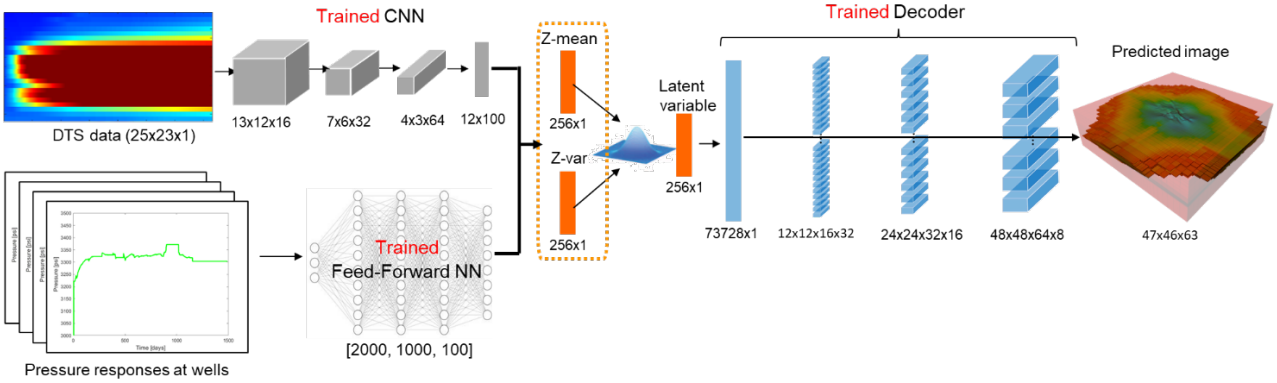

Figure 17. Neural network architecture: prediction

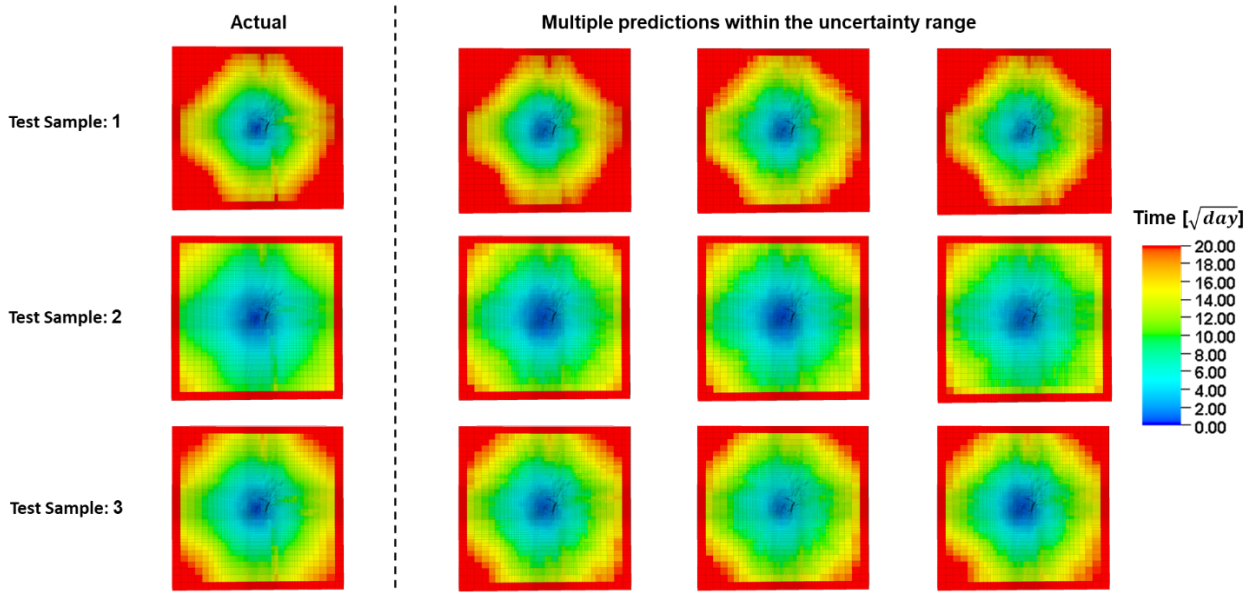

Figure 18. Prediction of DTOF map in blind test.

Reservoir model calibration and prediction of CO2 plume propagation

After validating the prediction accuracy of the trained neural network, the observed BHP of injector, behind-casing pressure of monitoring well, and DTS data along injector are fed into the trained neural network. The regression part of the neural network model provides the low dimensional latent variables

corresponding to the field DTOF map. By selecting several training and validation samples having close latent variables to the estimated target latent variables based on field monitoring data, we can obtain an ensemble of calibrated reservoir models. These models can be considered as history matched reservoir models. **Figure 19** shows the comparison of the well pressure responses and DTS data along the injector between prior ensemble (500 samples), posterior ensemble (10 nearest neighbors), and observed data. The history matching is implemented with 2 years historical data, and the following 2 years is considered as prediction period. The first observation is that posterior ensemble improved the matching performance with observed data over the prior ensembles for both history matching period and prediction period. The second observation is that the uncertainty of ensemble is reduced after history matching as expected. For the DTS data, reasonable agreement is confirmed after the history matching process from cross plot in **Figure 19**. Overall, in all observed data, a reasonable matching performance is confirmed, which validates the ability of the proposed history matching workflow. Compared with the traditional history matching workflow such as genetic algorithms, the selection of posterior models can be done rapidly (model selection can be done by a few seconds) in the proposed deep learning-based workflow, and significant acceleration is obtained while maintaining reasonable accuracy.

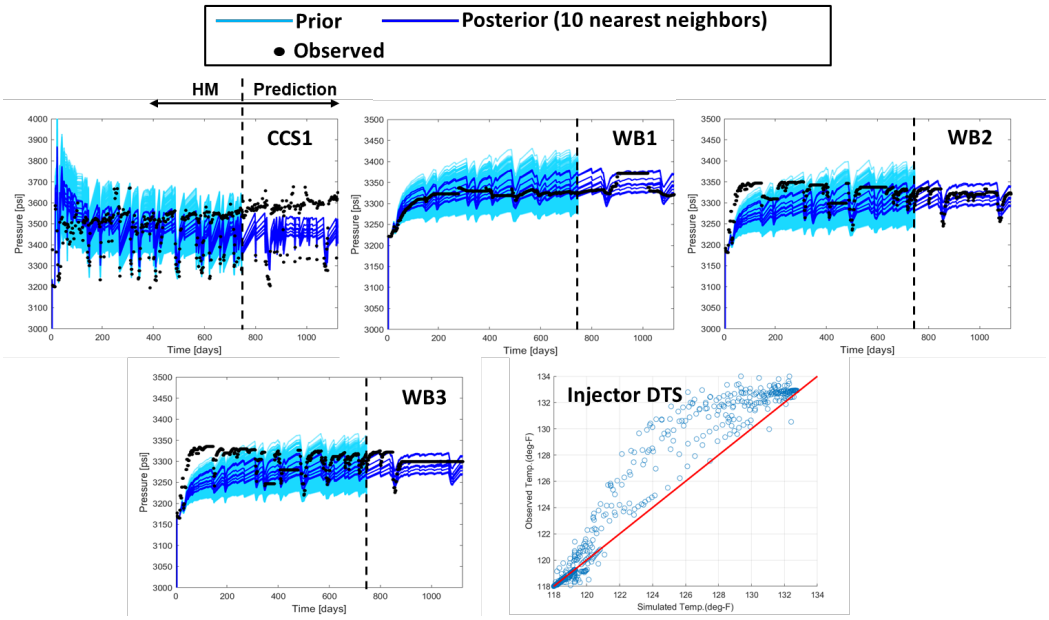

Figure 19. Comparison of pressure responses and DTS data between calibrated models and observed data.

Finally, CO2 saturation evolution is predicted by running the numerical simulation of these calibrated reservoir models. The simulation results of two nearest neighbor models are shown in **Figure 20**. In this simulation, CO2 is injected from 2011-11-1 to 2014-11-27, and the behavior of CO2 plume evolution until 2015-12-1 (1 year of post-injection period) is simulated. **Figure 20** shows the CO2 saturation evolution with respect to time. The predicted CO2 plume propagation images can be used for CO2 leakage analysis and for optimizing the CO2 sequestration operation.

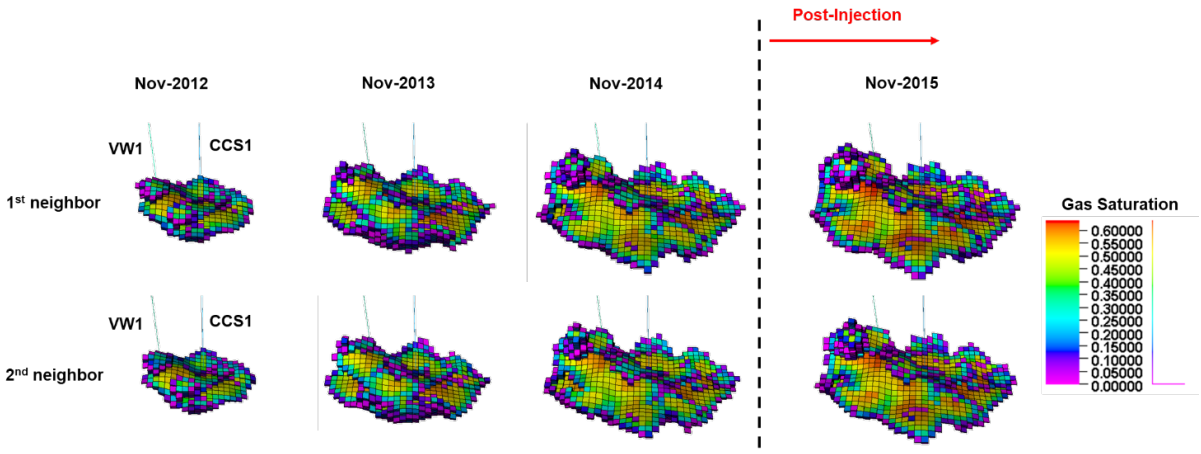

Figure 20. CO2 evolution with time by calibrated models.

Conclusions

- An efficient deep learning-based workflow for data assimilation has been developed for CO2 sequestration operation. Diffusive time of flight (DTOF) map is used for input and output of variational autoencoder (VAE) as a representative reservoir image. The use of DTOF provides two benefits: 1. Dimensionality reduction compared with snapshots of pressure or saturation images at different timesteps, 2. Computational time is reduced because the DTOF images can be efficiently calculated using FMM without numerical simulation. These benefits improve the efficiency of the neural network training and reduce the computational cost for the training data generation.
- The proposed workflow has been applied to a large-scale CO2 sequestration project, the Illinois Basin – Decatur Project (IBDP). The DTOF map was predicted from sparse observed data: the injector bottom-hole pressure, the behind-casing pressure at the monitoring well, and DTS data along the injector. Also, the characteristic of the VAE latent space enables us to select multiple calibrated reservoir models, and CO2 plume evolution can be predicted by running simulations of the selected models.
- In the field application, the main challenge was the computational time of the multi-component non-isothermal simulation (600 hours with a single core). To resolve this challenge, upscaling of the geologic model is applied, which properly considers the tradeoff between the model accuracy and computational efficiency. Because the DTOF map can be generated without running numerical simulation, the DTOF maps are generated using original fine-scale models. As a result, the computational time of single forward simulation was reduced from 600 hours to 7 hours, which provides significant acceleration of training data generation.
- To accelerate the workflow further, it is promising to incorporate Fast Marching Method (FMM)-based rapid simulation for generating training data generation as potential future work. In FMM-based rapid simulation, the 1D spatial coordinate determined based on DTOF contour is used for flow simulation.

Acknowledgements

This work is partly supported by the U.S. Department of Energy initiative on Science Informed Machine Learning for Accelerating Real Time Decisions for Subsurface Applications (SMART) and Texas A&M Joint Industry Project ‘Model Calibration and Efficient Reservoir Imaging (MCERI). The views and opinions of authors expressed herein do not necessarily state or reflect those of the United States Government or any agency thereof.

References

Aminu, Mohammed D., Nabavi, Seyed Ali, Rochelle, Christopher A. et al. 2017. A review of developments in carbon dioxide storage. *Applied Energy* **208**: 1389-1419. https://www.sciencedirect.com/science/article/pii/S0306261917313016.

Bandilla, Karl W., Celia, Michael A., and Leister, Evan. 2014. Impact of Model Complexity on CO2 plume modeling at Sleipner. *Energy Procedia* **63**: 3405-3415. https://www.sciencedirect.com/science/article/pii/S1876610214021845.

Benson, Sally M. and Myer, L. 2003. Monitoring to ensure safe and effective geologic sequestration of carbon dioxide. *Proc.,* Workshop on carbon dioxide capture and storage Proceedings, Netherlands178. http://inis.iaea.org/search/search.aspx?orig_q=RN:34028843.

Chen, Bailian, Harp, Dylan R., Lin, Youzuo et al. 2018. Geologic CO2 sequestration monitoring design: A machine learning and uncertainty quantification based approach. *Applied Energy* **225**: 332-345. https://www.sciencedirect.com/science/article/pii/S0306261918307372.

Chen, Hongquan, Sen, Deepthi, Datta-Gupta, Akhil et al. 2021. Model-Free Assessment of Inter-Well Connectivity in CO2 WAG Projects Using Statistical Recurrent Unit Models. *Proc.,* SPE Annual Technical Conference and Exhibition. https://doi.org/10.2118/205944-MS.

Chen, Hongquan, Terada, Kazuyuki, Li, Ao et al. 2022. Rapid Simulation of Unconventional Reservoirs Using Multi-Domain Multi-Resolution Discretization Based on the Diffusive Time of Flight. *Proc.,* SPE/AAPG/SEG Unconventional Resources Technology Conference. https://doi.org/10.15530/urtec-2022-3723026.

Datta-Gupta, A. and King, Michael. 2007. *Streamline Simulation: Theory and Practice*, Vol. 11.

Datta-Gupta, Akhil, Xie, Jiang, Gupta, Neha et al. 2011. Radius of Investigation and its Generalization to Unconventional Reservoirs. *Journal of Petroleum Technology* **63** (07): 52-55. https://doi.org/10.2118/0711-0052-JPT.

Guo, Bo, Bandilla, Karl W., Doster, Florian et al. 2014. A vertically integrated model with vertical dynamics for CO2 storage. *Water Resources Research* **50** (8): 6269-6284. https://agupubs.onlinelibrary.wiley.com/doi/abs/10.1002/2013WR015215.

Iino, Atsushi, Onishi, Tsubasa, and Datta-Gupta, Akhil. 2020. Optimizing CO2- and Field-Gas-Injection EOR in Unconventional Reservoirs Using the Fast-Marching Method. *SPE Reservoir Evaluation & Engineering* **23** (01): 261-281. https://doi.org/10.2118/190304-PA.

Jeong, Hoonyoung and Srinivasan, Sanjay. 2016. Fast assessment of CO2 plume characteristics using a connectivity based proxy. *International Journal of Greenhouse Gas Control* **49**: 387-412. https://www.sciencedirect.com/science/article/pii/S1750583616300962.

Jia, Bao, Tsau, Jyun-Syung, and Barati, Reza. 2018. Role of molecular diffusion in heterogeneous, naturally fractured shale reservoirs during CO2 huff-n-puff. *Journal of Petroleum Science and Engineering* **164**: 31-42. https://www.sciencedirect.com/science/article/pii/S0920410518300354.

Kingma, Diederik P and Welling, Max. 2013. Auto-Encoding Variational Bayes. https://ui.adsabs.harvard.edu/abs/2013arXiv1312.6114K.

Kingma, Diederik P. and Ba, Jimmy. 2014. Adam: A Method for Stochastic Optimization. https://ui.adsabs.harvard.edu/abs/2014arXiv1412.6980K.

Mathias, Simon A., Hardisty, Paul E., Trudell, Mark R. et al. 2008. Approximate Solutions for Pressure Buildup During CO2 Injection in Brine Aquifers. *Transport in Porous Media* **79** (2): 265. https://doi.org/10.1007/s11242-008-9316-7.

Michael, K., Golab, A., Shulakova, V. et al. 2010. Geological storage of CO2 in saline aquifers—A review of the experience from existing storage operations. *International Journal of Greenhouse Gas Control* **4** (4): 659-667. https://www.sciencedirect.com/science/article/pii/S1750583610000071.

Mo, Shaoxing, Zhu, Yinhao, Zabaras, Nicholas et al. 2019. Deep Convolutional Encoder-Decoder Networks for Uncertainty Quantification of Dynamic Multiphase Flow in Heterogeneous Media.

Water Resources Research **55** (1): 703-728. https://agupubs.onlinelibrary.wiley.com/doi/abs/10.1029/2018WR023528.

Møll Nilsen, Halvor, Herrera, Paulo A., Ashraf, Meisam et al. 2011. Field-case simulation of CO2 -plume migration using vertical-equilibrium models. *Energy Procedia* **4**: 3801-3808. https://www.sciencedirect.com/science/article/pii/S1876610211005947.

Nagao, Masahiro, Datta-Gupta, Akhil, Onishi, Tsubasa et al. 2023. Reservoir Connectivity Identification and Robust Production Forecasting Using Physics Informed Machine Learning. *Proc.,* SPE Reservoir Simulation Conference. https://doi.org/10.2118/212201-MS.

Nagao, Masahiro, Yao, Changqing, Onishi, Tsubasa et al. 2022. An Efficient Deep Learning-Based Workflow for CO2 Plume Imaging Using Distributed Pressure and Temperature Measurements. *Proc.,* SPE Annual Technical Conference and Exhibition. https://doi.org/10.2118/210309-MS.

Nagao, Masahiro, Yao, Changqing, Onishi, Tsubasa et al. 2023. An Efficient Deep Learning-Based Workflow for CO2 Plume Imaging With Distributed Pressure and Temperature Measurements. *SPE Journal* **28** (06): 3224-3238. https://doi.org/10.2118/210309-PA.

Nagao, Masahiro, Yao, Changqing, Onishi, Tsubasa, Chen, Hongquan, Datta-Gupta, Akhil and Mishra, Srikanta. 2022. An Efficient Deep Learning-Based Workflow for CO2 Plume Imaging Considering Model Uncertainties Using Distributed Pressure and Temperature Measurements. Paper presented at the 16th Greenhouse Gas Control Technologies Conference (GHGT-16), Lyon, France, 23-24 Oct 2022. Available at SSRN: https://ssrn.com/abstract=4280048 or http://dx.doi.org/10.2139/ssrn.4280048.

Nilsen, Halvor Møll, Lie, Knut-Andreas, and Andersen, Odd. 2016. Robust simulation of sharp-interface models for fast estimation of CO2 trapping capacity in large-scale aquifer systems. *Computational Geosciences* **20** (1): 93-113. https://doi.org/10.1007/s10596-015-9549-9.

Nordbotten, Jan Martin, Celia, Michael A., and Bachu, Stefan. 2005. Injection and Storage of CO2 in Deep Saline Aquifers: Analytical Solution for CO2 Plume Evolution During Injection. *Transport in Porous Media* **58** (3): 339-360. https://doi.org/10.1007/s11242-004-0670-9.

Olalotiti-Lawal, Feyi, Onishi, Tsubasa, Datta-Gupta, Akhil et al. 2019. Model calibration and optimization of a post-combustion CO2 WAG pilot in a mature oil field. *Fuel* **255**: 115810. https://www.sciencedirect.com/science/article/pii/S0016236119311627.

Onishi, Tsubasa, Chen, Hongquan, Datta-Gupta, Akhil et al. 2021. An Efficient Deep Learning-Based Workflow Incorporating a Reduced Physics Model for Subsurface Imaging in Unconventional Reservoirs. *Proc.,* SPE Annual Technical Conference and Exhibition. https://doi.org/10.2118/206065-MS.

Onishi, Tsubasa, Nguyen, Minh C., Carey, J. William et al. 2019. Potential CO2 and brine leakage through wellbore pathways for geologic CO2 sequestration using the National Risk Assessment Partnership tools: Application to the Big Sky Regional Partnership. *International Journal of Greenhouse Gas Control* **81**: 44-65. https://www.sciencedirect.com/science/article/pii/S1750583618302329.

Sen, Deepthi, Chen, Hongquan, and Datta-Gupta, Akhil. 2022. Inter-well connectivity detection in CO2 WAG projects using statistical recurrent unit models. *Fuel* **311**: 122600. https://www.sciencedirect.com/science/article/pii/S0016236121024674.

Sethian, J. A. 1999. Fast Marching Methods. *SIAM Review* **41** (2): 199-235. https://doi.org/10.1137/S0036144598347059

http://dx.doi.org/10.1137/S0036144598347059.

Sharma, Susan Sunila. 2011. Determinants of carbon dioxide emissions: Empirical evidence from 69 countries. *Applied Energy* **88** (1): 376-382. https://www.sciencedirect.com/science/article/pii/S0306261910002916.

Shokouhi, Parisa, Kumar, Vikas, Prathipati, Sumedha et al. 2021. Physics-informed deep learning for prediction of CO2 storage site response. *Journal of Contaminant Hydrology* **241**: 103835. https://www.sciencedirect.com/science/article/pii/S0169772221000747.

Song, Juan and Zhang, Dongxiao. 2013. Comprehensive Review of Caprock-Sealing Mechanisms for Geologic Carbon Sequestration. *Environmental Science & Technology* **47** (1): 9-22. https://doi.org/10.1021/es301610p.

Tanaka, Shusei, Datta-Gupta, Akhil, and King, Michael J. 2014. Compositional Streamline Simulation of CO2 Injection Accounting for Gravity and Capillary Effects Using Orthogonal Projection. *Proc.,* SPE Improved Oil Recovery Symposium. https://doi.org/10.2118/169066-MS.

Tang, Hewei, Fu, Pengcheng, Sherman, Christopher S. et al. 2021. A Deep Learning-Accelerated Data Assimilation and Forecasting Workflow for Commercial-Scale Geologic Carbon Storage. https://ui.adsabs.harvard.edu/abs/2021arXiv210509468T.

Tang, Meng, Liu, Yimin, and Durlofsky, Louis J. 2021. Deep-learning-based surrogate flow modeling and geological parameterization for data assimilation in 3D subsurface flow. *Computer Methods in Applied Mechanics and Engineering* **376**: 113636. https://www.sciencedirect.com/science/article/pii/S0045782520308215.

Vasco, D. W., Yoon, Seongsik, and Datta-Gupta, Akhil. 1999. Integrating Dynamic Data Into High-Resolution Reservoir Models Using Streamline-Based Analytic Sensitivity Coefficients. *SPE Journal* **4** (04): 389-399. https://doi.org/10.2118/59253-PA.

Viebahn, Peter, Vallentin, Daniel, and Höller, Samuel. 2015. Prospects of carbon capture and storage (CCS) in China's power sector – An integrated assessment. *Applied Energy* **157**: 229-244. https://www.sciencedirect.com/science/article/pii/S0306261915008521.

Wade Zaluski, Si-Yong Lee. 2021. 2020 IBDP Final Static Geological Model Development and Dynamic Modelling, Schlumberger (July 18, 2021).

Wen, Gege, Li, Zongyi, Azizzadenesheli, Kamyar et al. 2022. U-FNO-An enhanced Fourier neural operator-based deep-learning model for multiphase flow. *Advances in Water Resources* **163**: 104180. https://ui.adsabs.harvard.edu/abs/2022AdWR..16304180W.

Wen, Gege, Li, Zongyi, Long, Qirui et al. 2022. Real-time high-resolution CO$_2$ geological storage prediction using nested Fourier neural operators. https://ui.adsabs.harvard.edu/abs/2022arXiv221017051W.

Wen, Gege, Tang, Meng, and Benson, Sally M. 2021. Towards a predictor for CO2 plume migration using deep neural networks. *International Journal of Greenhouse Gas Control* **105**: 103223. https://www.sciencedirect.com/science/article/pii/S1750583620306484.

Wilkin, Richard T. and DiGiulio, Dominic C. 2010. Geochemical Impacts to Groundwater from Geologic Carbon Sequestration: Controls on pH and Inorganic Carbon Concentrations from Reaction Path and Kinetic Modeling. *Environmental Science & Technology* **44** (12): 4821-4827. https://doi.org/10.1021/es100559j.

Yan, Bicheng, Harp, Dylan Robert, Chen, Bailian et al. 2021. *A Physics-Constrained Deep Learning Model for Simulating Multiphase Fl ow in 3D Heterogeneous Porous Media*: arXiv.

Yao, Changqing, Chen, Hongquan, Onishi, Tsubasa et al. 2021. Robust CO2 Plume Imaging Using Joint Tomographic Inversion of Distributed Pressure and Temperature Measurements. *Proc.,* SPE Annual Technical Conference and Exhibition. https://doi.org/10.2118/206249-MS.

Zhang, Yanbin, Bansal, Neha, Fujita, Yusuke et al. 2016. From Streamlines to Fast Marching: Rapid Simulation and Performance Assessment of Shale-Gas Reservoirs by Use of Diffusive Time of Flight as a Spatial Coordinate. *SPE Journal* **21** (05): 1883-1898. https://doi.org/10.2118/168997-PA.

Zhong, Zhi, Sun, Alexander Y., and Jeong, Hoonyoung. 2019. Predicting CO2 Plume Migration in Heterogeneous Formations Using Conditional Deep Convolutional Generative Adversarial Network. *Water Resources Research* **55** (7): 5830-5851. https://agupubs.onlinelibrary.wiley.com/doi/abs/10.1029/2018WR024592.

Zhou, Wenji, Wang, Tao, Yu, Yadong et al. 2016. Scenario analysis of CO2 emissions from China's civil aviation industry through 2030. *Applied Energy* **175**: 100-108. https://www.sciencedirect.com/science/article/pii/S0306261916305864.